JVST A
Journal of Vacuum Science & Technology A

ARTICLE

avs.scitation.org/journal/jva

Thermal atomic layer etching of germanium-rich SiGe using an oxidation and "conversion-etch" mechanism

Cite as: J. Vac. Sci. Technol. A **39**, 022602 (2021); doi: 10.1116/6.0000834
Submitted: 2 December 2020 · Accepted: 29 January 2021 ·
Published Online: 24 February 2021

View Online Export Citation CrossMark

Aziz I. Abdulagatov,[1] Varun Sharma,[2,3] Jessica A. Murdzek,[1] Andrew S. Cavanagh,[1] and Steven M. George[1]

AFFILIATIONS

[1]Department of Chemistry, University of Colorado, Boulder, Colorado 80309-0215
[2]ASM Microchemistry Oy, Pietari Kalmin katu 3 F2, 00560 Helsinki, Finland
[3]Department of Chemistry, University of Helsinki, FI-00014 Helsinki, Finland

Note: This paper is part of the 2021 Special Topic Collection on Atomic Layer Etching (ALE).

ABSTRACT

The thermal atomic layer etching (ALE) of germanium-rich SiGe was demonstrated using an oxidation and "conversion-etch" mechanism with oxygen (O_2) or ozone (O_3), hydrofluoric acid (HF), and trimethylaluminum [TMA, $Al(CH_3)_3$] as the reactants. The crystalline germanium-rich SiGe film was prepared using physical vapor deposition and had a composition of $Si_{0.15}Ge_{0.85}$. *In situ* spectroscopic ellipsometry was employed to monitor the thickness of both the SiGe film and the surface oxide layer on the SiGe film during thermal ALE. Using a reactant sequence of O_2-HF-TMA, the etch rate of the SiGe film increased progressively with temperatures from 225 to 290 °C. At 290 °C, the SiGe film thickness decreased linearly at a rate of 0.57 Å/cycle with a surface oxide thickness of 18–19 Å. This etch rate was obtained using reactant pressures of 25, 0.2, and 0.4 Torr and doses of 1.5, 1.0, and 1.0 s for O_2, HF, and TMA, respectively. The TMA and HF reactions were self-limiting and the O_2 reaction was reasonably self-limiting at 290 °C. Using an O_3-HF-TMA reaction sequence, the SiGe ALE etch rate was 0.42 Å/cycle at 290 °C. This etch rate was obtained using reactant pressures of 15, 0.2, and 0.4 Torr and dose times of 0.5, 1.0, and 1.0 s for O_3, HF, and TMA, respectively. The O_3, TMA, and HF reactions were all self-limiting at 290 °C. Atomic force microscopy images revealed that thermal ALE with the O_2-HF-TMA or O_3-HF-TMA reaction sequences did not roughen the surface of the SiGe film. The SiGe film was etched selectively compared with Si or Si_3N_4 at 290 °C using an O_2-HF-TMA reaction sequence. The etch rate for the SiGe film was >10 times faster than Si(100) or Si_3N_4 that was prepared using low-pressure chemical vapor deposition. This selectivity for the SiGe film will be useful to fabricate Si nanowires and nanosheets using SiGe as the sacrificial layer.

I. INTRODUCTION

The continuous scaling of device dimensions has motivated the semiconductor industry to develop advanced process technologies. In recent years, atomic layer deposition (ALD) and atomic layer etching (ALE) have emerged as important processing techniques for miniaturization.[1,2] ALD is a deposition technique that is based on sequential, self-limiting surface reactions.[1] ALE is an etching technique that allows the removal of material from the surface in a layer-by-layer manner.[2] ALE can be based on either plasma[2] or thermal[3,4] sequential reactions that utilize surface modification and removal steps.

Plasma ALE utilizes a surface modification step typically involving halogen adsorption.[2] The surface-modified layer is then removed by a sputtering process with ions or energetic neutrals.[2] The directionality of the ions or energetic neutrals results in anisotropic etching.[2,5] In contrast, thermal ALE employs self-limiting, sequential thermal surface reactions.[3,4,6] Multiple mechanisms exist for thermal ALE based on surface modification and volatile release of the surface-modified layer.[3] The gas-phase thermal reactions etch isotropically in a layer-by-layer fashion.[3]

Processing advanced 3D device structures with atomic-level thickness control has continued to require ALD and ALE. Etching has

become more essential with the transition from planar to 3D devices. Both anisotropic and isotropic etching are necessary for the fabrication of future devices such as gate-all-around and nanosheet transistors.[7] Viewing 3D device fabrication like the construction of a skyscraper, anisotropic etching is used to form the vertical elevator shafts and isotropic etching is employed to form the horizontal hallways.

SiGe is a technologically important material with high carrier mobility that is needed for the fabrication of novel devices.[8,9] SiGe can be used in devices that require high electron mobility such as MOSFETs[8,10] and nanowire transistors.[11] SiGe also has properties that are useful for FinFETs,[12] Si/SiGe quantum dots,[13] direct bandgap emitters,[14] mid-infrared waveguides,[15] ultra-wideband photonics,[16] and MEMS devices.[17] The etching of SiGe is required for the fabrication of SiGe devices. In addition, SiGe is also used as a sacrificial layer in the formation of Si nanowires and nanosheets for nanotransistor structures.[7]

SiGe alloys can be etched using solution chemistries with $NH_4OH/H_2O_2/H_2O$[18] or $HF/H_2O_2/CH_3COOH$.[19] SiGe alloys can also be etched using chemical vapor etching with gas-phase HCl.[20–22] There are also many plasma approaches for SiGe etching using various plasma gases, such as CF_4, O_2, and HBr.[23–26] Many of these SiGe etching approaches can provide selective etching of SiGe in the presence of Si needed for the formation of Si nanowires and nanosheets.[7] However, there have been no previous reports of SiGe thermal ALE.

In this paper, the thermal ALE of SiGe is reported utilizing sequential exposures of oxygen (O_2) or ozone (O_3), hydrogen fluoride (HF), and trimethyl aluminum [$Al(CH_3)_3$]. A schematic showing this sequence of exposures is displayed in Fig. 1. This procedure utilizes the oxidation and "conversion-etch" mechanism. O_2 or O_3 are used for oxidation of the SiGe. TMA converts SiGe oxide to Al_2O_3.[27] HF fluorinates the Al_2O_3 to AlF_3.[6,28] TMA also undergoes ligand-exchange with AlF_3 to remove the AlF_3 as volatile products.[29,30]

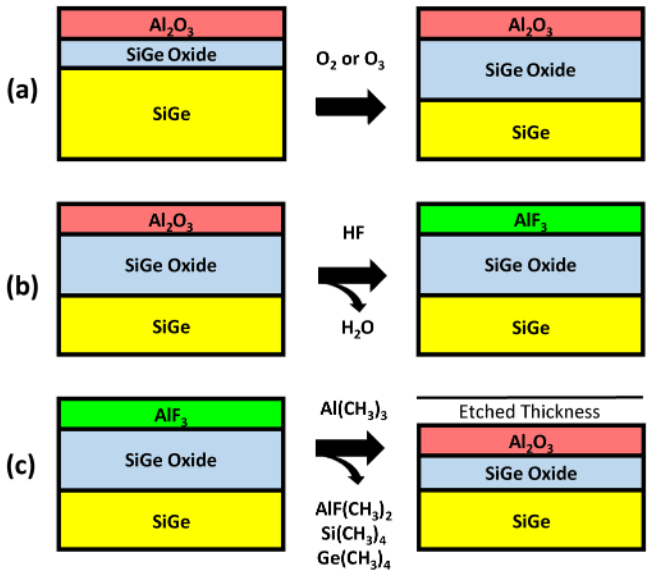

FIG. 1. Schematic for SiGe thermal ALE based on (a) oxidation by O_2 or O_3, (b) fluorination by HF, and (c) ligand-exchange and conversion by $Al(CH_3)_3$.

SiGe thermal ALE adds to the growing list of materials that can be etched using sequential, self-limiting thermal surface reactions.[3] Many of these thermal ALE systems involve the fluorination and ligand-exchange mechanism that is employed for Al_2O_3, HfO_2, and ZrO_2 ALE.[4,6,28,29,31–33] Other thermal ALE occurs via the conversion-etch mechanism that is used for SiO_2, ZnO, and WO_3 ALE.[27,34,35] The oxidation and conversion-etch mechanism is also applied for other Si-containing materials such as Si and Si_3N_4 thermal ALE.[36,37] In addition, the oxidation and conversion-etch mechanism can also define W ALE.[34]

II. EXPERIMENT

A. Reactor, *in situ* spectroscopic ellipsometry, and reactants

Thermal ALE of SiGe was conducted in a warm wall, hot-stage type reactor. A complete description of this apparatus has been presented earlier.[36] The walls of the reactor were maintained at 160 °C. The sample temperature was varied between 225 and 290 °C using a cartridge heater to heat the sample stage. The sample was held on the horizontal sample stage by gravity.

The reactor was equipped with an *in situ* spectroscopic ellipsometer (J.A. Woollam, model M-2000UI). Using this ellipsometer, the changes in the SiGe film thickness and the surface oxide layer were monitored in real-time during ALE. The model used to fit the ellipsometer results employed a stack of Woollam library files [SiO2_JAW/a-Ge_Adachi_cl/SiO2_JAW/INTRA_JAW(10 Å)/SiTempJAW]. Ellipsometric measurements were recorded after each ALE cycle during the purging step. The Al_2O_3 oxide layer was not explicitly considered in the model because the Al_2O_3 oxide layer is ultrathin and is merged with the SiO_2/GeO_2 layer.

One SiGe ALE cycle consisted of doses of O_2 or O_3, HF and TMA followed by a 30 s nitrogen purge time after each exposure, as illustrated in Fig. 1. Industrial grade O_2 (Airgas) was used for the oxidation. This O_2 was also the feed gas for the O_3 generator. The O_3 was produced by an ozone generator (O3ONIA, Switzerland) with an ozone output of ~15 wt. % relative to O_2. The HF-pyridine solution was used as the source of HF vapor.[31] HF-pyridine (70 wt. %) and trimethylaluminum (97%) were supplied by Sigma-Aldrich. Reported reactant pressures refer to their partial pressures with respect to the background N_2 gas pressure of ~1 Torr. Ultrahigh purity (UHP) grade N_2 (99.9999%, Airgas) was used as the carrier gas.

B. Samples and characterization

The sample consisted of a SiGe film with a thickness of 100 nm. This SiGe film was on a thermal SiO_2 layer with a thickness of 100 nm on a Si(100) wafer. The SiGe film was prepared using physical vapor deposition (PVD) and was supplied by Hionix Inc. Rutherford backscattering spectroscopy (RBS) analysis was used to obtain the composition of the SiGe film. The RBS results yielded a film composition of $Si_{0.15}Ge_{0.85}$. For simplicity in presenting the etching results, the $Si_{0.15}Ge_{0.85}$ film will also be described as the SiGe film.

Grazing incidence x-ray diffraction (GIXRD) analysis indicated that the $Si_{0.15}Ge_{0.85}$ films were crystalline. The GIXRD diffractogram is shown in Fig. 2(a). The GIXRD diffractogram displayed two broad peaks centered at 2Θ values of 27.4° and 49.5°. This diffraction peak pattern is typically observed for cubic polycrystalline SiGe or Ge.[38]

Raman spectral analysis was performed on the $Si_{0.15}Ge_{0.85}$ film using an excitation laser at 514.5 nm. The Raman spectrum is displayed in Fig. 2(b). The Raman spectrum shows the presence of Si–Si, Si–Ge, and Ge–Ge phonon modes located at 508.7, 370.9, and 273.7 cm^{-1}, respectively.[39] The existence of the Si–Ge peak indicates mixed Si–Ge bonding and no severe Si and Ge clustering. The broad diffraction peaks also are consistent with nanosized crystallites.

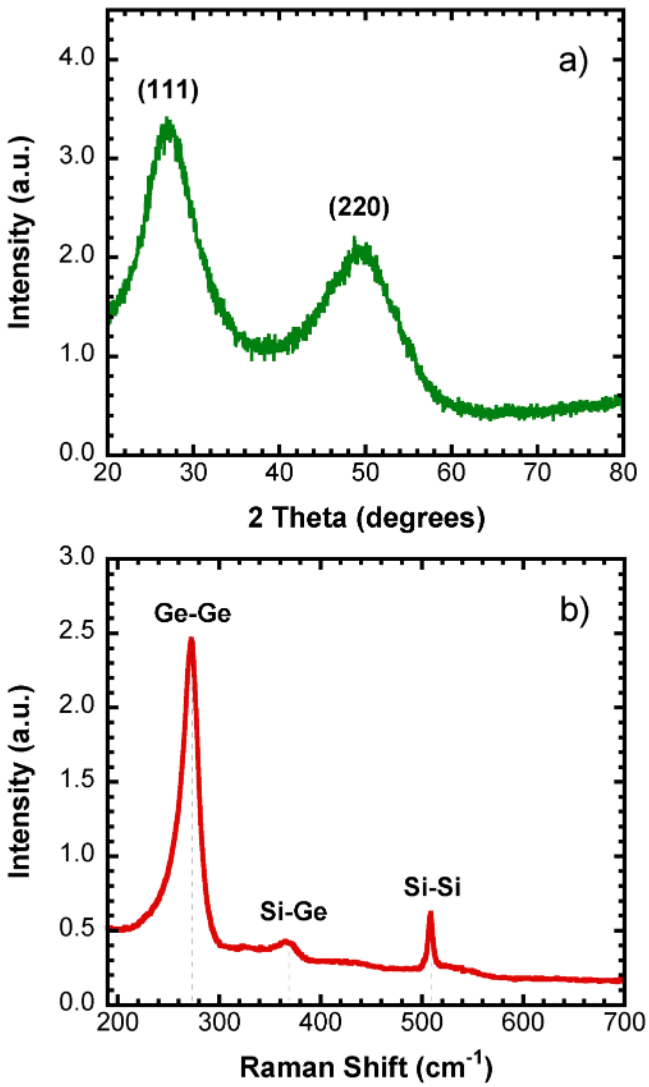

FIG. 2. (a) GIXRD diffractogram and (b) Raman spectra of as received PVD $Si_{0.15}Ge_{0.85}$ sample.

The selectivity experiments used low-pressure chemical vapor deposition (LPCVD) Si_3N_4 and a silicon-on-insulator (SOI) sample with a Si(100) layer. These samples were supplied by University Wafer Inc. The LPCVD Si_3N_4 samples had an initial thickness of 100 nm. RBS analysis of this film prior to ALE confirmed a Si-to-N ratio of 3-to-4. Forward recoil energy spectrometry (FRES) analysis detected hydrogen impurities in the Si_3N_4 films at <3 at. %. X-ray diffraction (XRD) analysis determined that the Si_3N_4 films were amorphous. The SOI sample had a 100 nm thick single-crystal Si(100) layer on a 2000 nm buried SiO_2 (BOX) film. The $Si_{0.15}Ge_{0.85}$, Si_3N_4, and SOI samples were 2 × 2 cm^2 coupons obtained from larger wafers.

X-ray photoelectron spectroscopy (XPS) was performed using a Thermo Scientific™ K-Alpha+ XPS system. XPS was used to map the surface film composition after the etch process. A monochromatic Al Kα x-ray source at 1486.6 eV was used to collect a survey scan as well as high-resolution scans for individual elements. The survey scan used a pass energy of 200 eV and a step size of 1 eV. The high-resolution scans were collected with a pass energy of 30 eV and a step size of 0.1 eV. The x-ray spot size was about 400 μm.

The XPS system was also equipped with a dual-beam flood gun for charge compensation. The Thermo Avantage v5.962 software package was employed to collect and analyze the data. The XPS detection limit was ~0.1 at. % and the fitting error was estimated to be around 0.5 at. %. The error in binding energies was ±0.1 eV. All the peaks were calibrated to the adventitious C 1s peak centered at 284.8 eV. An atomic force microscope (Nanosurf easyScan2) employing the tapping mode was used to measure the surface roughness before and after ALE.

III. RESULTS AND DISCUSSION

A. SiGe thermal ALE using O_2

Figure 3 shows the results for SiGe thermal ALE at 290 °C. The etching was performed using an O_2-HF-TMA reactant

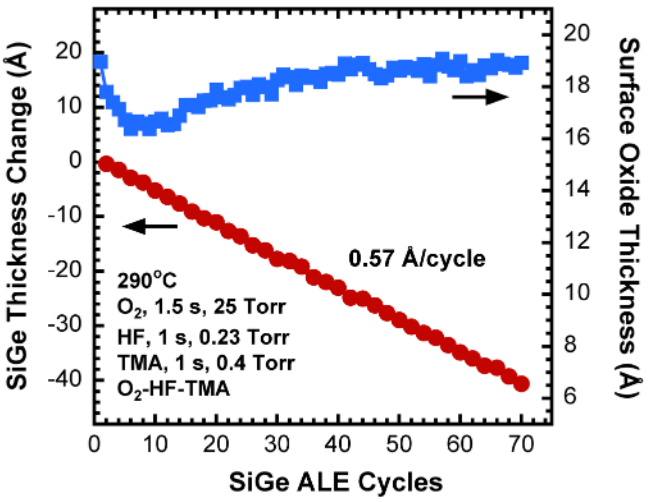

FIG. 3. SiGe thickness change and surface oxide film thickness vs number of ALE cycles using sequential exposures of O_2, HF, and TMA at 290 °C.

sequence where oxygen, hydrofluoric acid, and TMA were dosed for 1.5, 1, and 1 s, respectively. These doses of O_2, HF, and TMA produced partial pressures of 25, 0.23, and 0.4 Torr, respectively. The etch temperature of 290 °C was chosen to avoid potential problems with TMA decomposition that may occur at >300 °C.[40,41]

The linear decrease in the SiGe film thickness in Fig. 3 is consistent with an etch rate of 0.57 Å/cycle. The surface oxide layer thickness levels off at about 19 Å after 60 ALE cycles. Similar etching behavior was observed during Si(100) and LPCVD Si_3N_4 thermal ALE using the same reactants, sequence, and etch temperature.[36,37] However, in contrast to Si and Si_3N_4 thermal ALE, the $Si_{0.15}Ge_{0.85}$ film is etched without using high pressure, static reactant doses.

The ease of etching the SiGe films relative to etching the Si and Si_3N_4 films indicates that at least one of the reaction steps during SiGe thermal ALE is more favorable relative to Si or Si_3N_4 thermal ALE. Thermochemical calculations for the standard Gibbs free energy change for the oxidation of Si and Ge reveal that silicon oxidation is more favorable than germanium oxidation,[42]

$$\mathrm{Si} + \mathrm{O_2(g)} \rightarrow \mathrm{SiO_2}, \qquad \Delta G^\circ(300\,^\circ\mathrm{C}) = -193\ \mathrm{kcal}, \quad (1)$$

$$\mathrm{Ge} + \mathrm{O_2(g)} \rightarrow \mathrm{GeO_2}, \qquad \Delta G^\circ(300\,^\circ\mathrm{C}) = -112\ \mathrm{kcal}. \quad (2)$$

In contrast, the conversion of GeO_2 to Al_2O_3 is more favorable than the conversion of SiO_2 to Al_2O_3 using TMA,[42]

$$1.5\mathrm{SiO_2} + 2\mathrm{Al(CH_3)_3(g)} \rightarrow \mathrm{Al_2O_3} + 1.5\mathrm{Si(CH_3)_4(g)}, \qquad \Delta G^\circ(300\,^\circ\mathrm{C}) = -88\ \mathrm{kcal}, \quad (3)$$

$$1.5\mathrm{GeO_2} + 2\mathrm{Al(CH_3)_3(g)} \rightarrow \mathrm{Al_2O_3} + 1.5\mathrm{Ge(CH_3)_4(g)}, \qquad \Delta G^\circ(300\,^\circ\mathrm{C}) = -170\ \mathrm{kcal}. \quad (4)$$

The more facile etching of SiGe suggests that the conversion of GeO_2 may be the main factor determining the etch rate. In addition, oxidation of SiGe is enhanced compared with the separate oxidation of Si and Ge.[43,44] The Ge/GeO_2 interface also has low thermal stability. The Ge/GeO_2 interface can decompose to GeO upon heating.[45,46] However, GeO desorption is not reported at <400 °C.[45,47] The Al_2O_3 surface layer that forms during the conversion step during SiGe thermal ALE may also act as a capping layer, suppress GeO desorption and stabilize the oxidation process.[48]

B. Effect of reactant exposure

Figure 4 displays the change in SiGe etch rates versus dose times of O_2, TMA, and HF at 290 °C using the O_2-HF-TMA reactant sequence. Figure 4(a) shows the SiGe etch rates versus O_2 dose times. In this experiment, the dose times for TMA and HF were fixed at 1 s and the oxygen dose time was varied between 0.4 and 2.5 s. An increase in O_2 dose time resulted in a rise in O_2 partial pressure from 15 Torr for the 0.4 s dose to 30 Torr for the 2.5 s dose. The partial pressures of TMA and HF remained constant at 0.40 and 0.23 Torr, respectively. The SiGe etch rate increases with longer O_2 dose times.

Figure 4(b) shows the SiGe etch rates versus TMA dose times. The dose times for TMA were varied between 0.4 and 1.7 s. The partial pressure of TMA was about 0.40 Torr and stayed constant with increasing dose times. The O_2 and HF dose times were 1.5 and 1.0 s, respectively. The O_2 and HF partial pressures were 25 and 0.23 Torr, respectively. Figure 4(b) reveals that the TMA reaction is self-limiting at TMA dose times >0.4 s. Figure 4(c) displays the SiGe etch rates as a function of HF dose time. The O_2 and TMA doses were 1.5 and 1.0 s, respectively. The dose times for HF varied between 0.5 and 1.7 s. Figure 4(c) demonstrates that HF reaction is self-limiting at HF dose times >0.5 s.

C. Temperature dependence of etch rate

Figure 5 shows the SiGe etch rate dependence on temperature. These results were obtained using the O_2-HF-TMA reactant sequence at 225, 240, 260, 275, and 290 °C. The O_2, HF, and TMA dose times were 1.5, 1.0, and 1.0 s, respectively. These doses produced partial pressures of 25, 0.23, and 0.40 Torr for O_2, HF, and TMA, respectively. The etch rate increases from 0.07 Å/cycle at 225 °C to 0.57 Å/cycle at 290 °C. This increase in temperature is consistent with a thermally activated process. An Arrhenius plot of the temperature-dependent SiGe etch rates is shown in Fig. 6. An activation barrier of $E_a = 16.3$ kcal/mol is derived for the combined oxidation, conversion, fluorination, and ligand-exchange reactions during SiGe thermal ALE.

Similar thermally activated etching was observed during Si(100) and LPCVD Si_3N_4 thermal ALE.[36,37] The thermal ALE of these silicon-containing materials was also performed using the oxidation and "conversion-etch" mechanism using O_2 or O_3, HF, and TMA. An activation barrier of $E_a = 13.4$ kcal/mol was measured for Si_3N_4 ALE.[37] The temperature-dependent etching of Si(100) was only performed for three different temperatures.[36] These temperatures yield an activation barrier of $E_a = 6.0$ kcal/mol. The variation between these activation barriers for SiGe, Si_3N_4, and Si etching may be attributed to the different substrate compositions and reaction parameters. SiGe substrate is Ge-rich with a composition of $Si_{0.15}Ge_{0.85}$. The SiGe etching was also performed at lower O_2 pressures. In addition, the etching of Si_3N_4 and Si was conducted using static pressures compared with viscous flow conditions for SiGe etching.

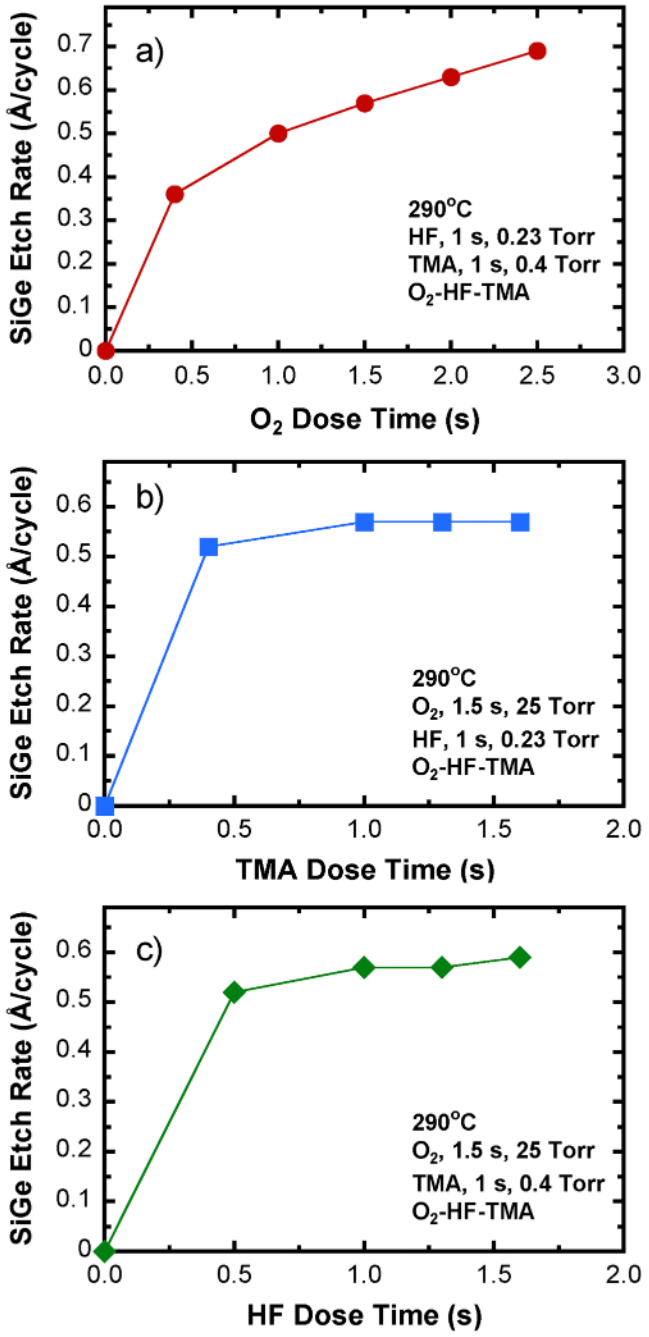

FIG. 4. SiGe etch rate vs (a) O_2, (b) TMA, and (c) HF dose times at 290 °C.

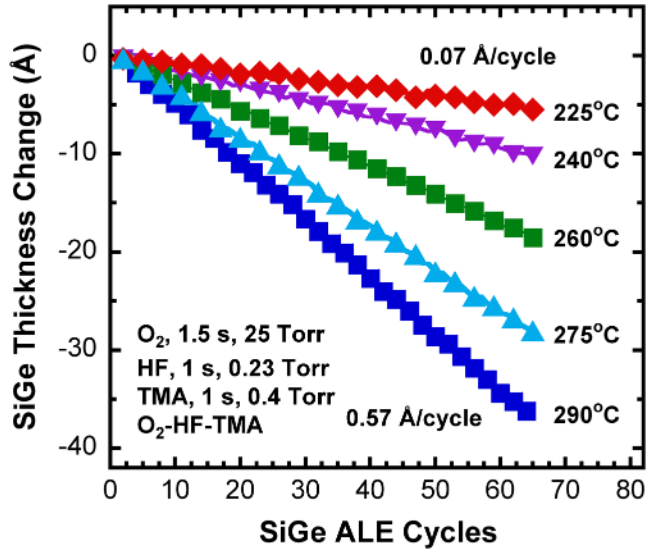

FIG. 5. SiGe thickness change vs number of ALE cycles at various temperatures.

D. Surface roughness and composition after etching

Figure 7 shows AFM images with dimensions of $10 \times 10\,\mu$m of the $Si_{0.15}Ge_{0.85}$ film surface before and after 100 ALE cycles. The etching was performed at 290 °C using the O_2-HF-TMA reactant sequence with O_2, HF, and TMA dose times of 1.5, 1.0, and 1.0 s, respectively. The root-mean-square (RMS) surface roughness of the $Si_{0.15}Ge_{0.85}$ film in Fig. 7(a) prior to etching is 8.3 ± 0.2 Å. The AFM image reveals a few surface irregularities such as pinholes. Small voids have also been observed on the surface of other sputtered SiGe films.[49] These voids should not be present on the surface of epitaxial SiGe films that would be used for device fabrication.[50]

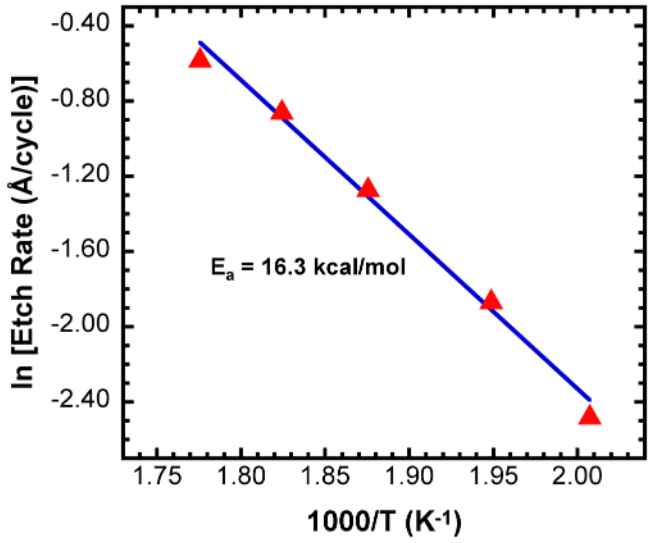

FIG. 6. Arrhenius plot of the temperature-dependent SiGe etch rates.

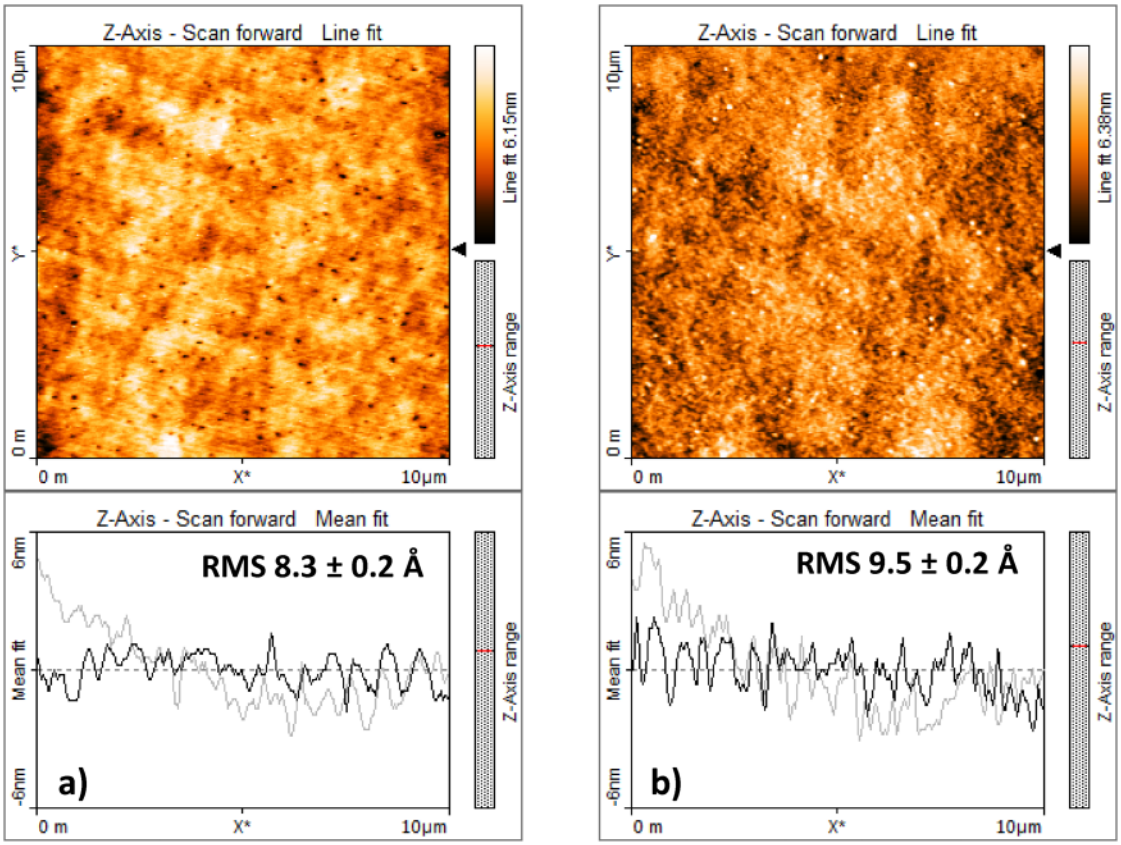

FIG. 7. AFM image of $Si_{0.15}Ge_{0.85}$ film surface (a) before and (b) after 100 ALE cycles using the O_2-HF-TMA dose sequence at 290 °C.

Figure 7(b) shows the corresponding surface topography after 100 ALE cycles. The RMS roughness for the etched sample increases slightly to 9.5 ± 0.2 Å. This result is similar to the results for the thermal ALE of Si(100) and LPCVD Si_3N_4 where no significant change in roughness was observed after ALE.[36,37] The AFM image in Fig. 7(b) also observes some small nanoparticles evenly spread on the surface. Additional AFM measurements determined that the average size of these nanoparticles was ~100 nm. Attempts to determine the identity of these nanoparticles using energy dispersive spectroscopy (EDS) were not successful.

Ex situ XPS analyses were performed to determine the surface elemental composition of the $Si_{0.15}Ge_{0.85}$ film before and after 100 ALE cycles with the O_2-HF-TMA reactant sequence at 290 °C. The $Si_{0.15}Ge_{0.85}$ surface prior to etching had a composition of 38.8, 50.9, 5.2, and 5.1 at. % for Ge, O, Si, and C, respectively. After 100 ALE cycles ending with a TMA dose and subsequent atmospheric exposure, the surface of the $Si_{0.15}Ge_{0.85}$ film had a composition of 39.1, 29.4, 8.8, 20.9, 0.8, 1.0 at. % for Ge, O, Si, C, F, and Al, respectively. The small F and Al XPS signals are consistent with efficient ligand-exchange that nearly removes the AlF_3 surface layer after the TMA dose.

Figure 8(a) shows the high-resolution Ge 3d XPS spectra of $Si_{0.15}Ge_{0.85}$ before and after ALE. Both spectra reveal the Ge^0 $3d_{5/2}$ XPS peak at 29.4 eV. The prominent shoulder peak centered near 33.5 ± 0.1 eV before ALE can be assigned to the $SiGeO_x$ mixed oxide.[51] This XPS peak is much smaller after ALE. The decrease of this XPS peak is consistent with the reduction of the surface oxide after ALE. As shown in Fig. 3, the $Si_{0.15}Ge_{0.85}$ film has a native oxide with a thickness of ~31 Å before ALE. The thickness of the surface oxide decreases to ~19 Å after ALE.

There are also shoulder XPS peaks at a lower intensity in Fig. 8(a) that are attributed to Ge in the 1+, 2+, 3+, and 4+ oxidation states. The chemical shifts of Ge^{1+}, Ge^{2+}, Ge^{3+}, and Ge^{4+} relative to Ge^0 have been reported as 0.8, 1.8, 2.75, and 3.3 eV, respectively.[52–54] The dashed lines show the binding energies for these Ge oxidation states. The various Ge oxidation states are different before and after ALE. The low amount of the Ge oxidation after ALE could be explained by GeO_2 reduction by TMA during the conversion step. Previous studies have revealed the partial reduction of GeO_2 after Al_2O_3 ALD using TMA and H_2O as the reactants at 300 °C.[55]

Figure 8(b) displays the Si 2p XPS spectra of the $Si_{0.15}Ge_{0.85}$ film before and after ALE. The peak at 99.5 eV is assigned to the Si

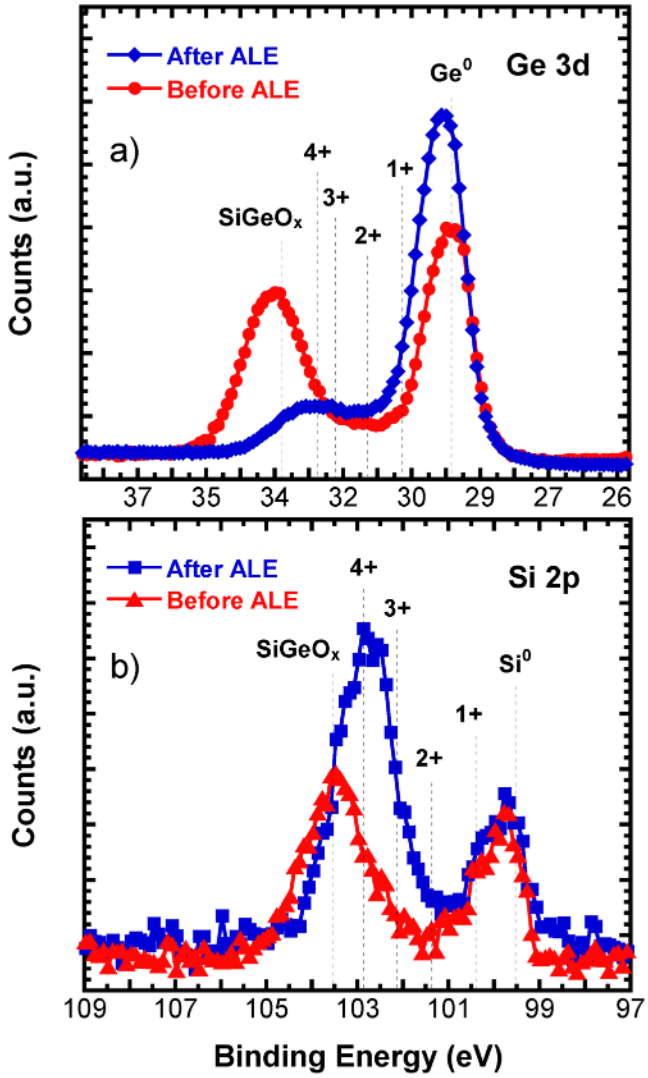

FIG. 8. XPS spectrum of (a) Ge 3d, and (b) Si 2p signals for $Si_{0.15}Ge_{0.85}$ sample before and after 100 cycles of ALE at 290 °C using O_2-HF-TMA sequence.

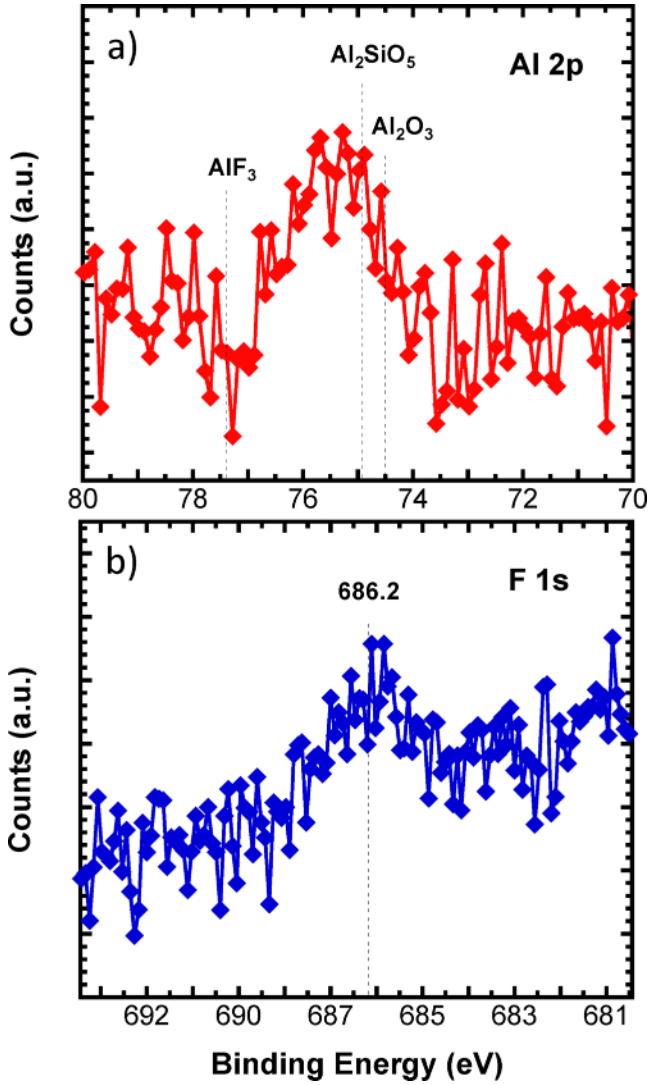

FIG. 9. XPS spectrum of (a) Al 2p and (b) F 1 s signals for $Si_{0.15}Ge_{0.85}$ sample after 100 cycles of ALE at 290 °C using O_2-HF-TMA sequence.

$2p_{3/2}$ XPS peak of elemental Si. Before ALE, there is also a Si 2p XPS peak around 103.5 eV corresponding to surface $SiGeO_x$.[51] After ALE, there is a high-intensity Si 2p shoulder peak at about 102.9 eV. The dashed lines in Fig. 8(b) show the binding energies for elemental Si and various silicon oxidation states from 4+ to 1 +. The chemical shifts of Si^{1+}, Si^{2+}, Si^{3+}, and Si^{4+} relative to Si^0 have been reported as 0.9, 1.9, 2.6, and 3.4 eV, respectively.[56,57] The high-intensity Si 2p shoulder peak after ALE is assigned to the Si^{4+} oxidation state.

There are also changes in the lower oxidation states of Si in the $Si_{0.15}Ge_{0.85}$ film before and after ALE. The Si^{2+} and Si^{3+} oxidation states are much more prominent after ALE. Oxidation during ALE converts Si to SiO_2. The higher intensity silicon suboxides may be attributed to the reduction of SiO_2 from Si^{4+} to Si suboxides by TMA. SiO_2 reduction has been observed previously during SiO_2 ALE using TMA and HF.[27] The presence of Ge should not shift the Si XPS peaks nor should the presence of Si affect the Ge XPS peaks.[58,59] In addition, SiO_xF_y could be formed by the HF fluorination step during ALE.[27] SiO_xF_y species have a Si $2p_{3/2}$ XPS peak at 102.8 ± 0.4 eV.[60]

Figure 9 shows high-resolution XPS spectra for Al 2p and F 1 s from the $Si_{0.15}Ge_{0.85}$ film after 100 ALE cycles. Figure 9(a) shows that the Al 2p XPS peak is observed at 75.4 eV. This binding energy is higher than ~74.5 eV for Al_2O_3[61] and lower than ~77.3 eV for AlF_3.[61] The binding energy of 75.4 eV is fairly close to

the binding energy of 74.9 eV for aluminosilicate (Al_2SiO_5).[62] The binding energy of 75.4 eV for the Al 2p XPS peak in Fig. 9(a) is consistent with an AlO_xF_y species.[63–65]

The F 1 s spectra in Fig. 9(b) exhibits a maximum located around 686.2 eV. This binding energy is in agreement with the fluoride peak expected for SiF or GeF surface species.[66] Since Fig. 9(b) did not display an Al 2p peak with binding energy as high as ~77.0 eV for AlF_3,[63] there is probably no AlF_3 on the surface. These results argue that the ligand-exchange reaction with TMA must remove the AlF_3 surface species after the previous fluorination reaction.[27] The remaining F species are most likely $SiGeO_xF_y$ species.

E. Removal of residual surface oxide

SiGe thermal ALE involves the formation of a surface oxide layer. This oxide layer remains on the surface after ALE. In previous work on the thermal ALE of Si-containing materials, the surface oxide on Si or Si_3N_4 after ALE has been removed using sequential HF and TMA exposures.[36,37] This approach is based on the SiO_2 thermal ALE process.[27]

Figure 10 displays the surface oxide thickness and the SiGe film thickness change during 40 sequential cycles of TMA and HF at 290 °C. These cycles were performed after SiGe ALE with O_2, HF, and TMA sequential exposures. The etching was performed using TMA doses of 1 s and HF doses of 0.7 s. There was a 30 s purge time between the HF and TMA doses. Partial pressures of TMA and HF were 1.2 and 0.4 Torr, respectively.

Figure 10 shows that the surface oxide thickness is rapidly decreased from ~14 to 5 Å in the first 6 oxide ALE cycles. The surface oxide thickness is then apparently unchanged over the next 34 oxide ALE cycles. Similar behavior was observed during surface oxide removal using TMA and HF after the thermal ALE of Si(100) and LPCVD Si_3N_4.[36,37] The true oxide thickness may be negligible because the apparent oxide thickness obtained from the ellipsometry analysis may be associated with surface roughness.[67,68] Figure 10 also reveals that the SiGe film thickness is nearly constant during the surface oxide removal.

F. Effect of precursor exposure sequence

The precursor dose sequence may affect the SiGe etch rate. Figure 11 compares SiGe thickness change versus number of ALE cycles for O_2-HF-TMA and O_2-TMA-HF dose sequences at 290 °C. The O_2, HF, and TMA reactants were dosed for 1.5, 1.0, and 1.0 s, respectively, with a 30 s purge in between each reactant dose. Figure 11 shows that the O_2-TMA-HF sequence slightly lowers the etch rate to 0.45 Å/cycle compared with the etch rate of 0.57 Å/cycle for the O_2-HF-TMA sequence.

Similar results were obtained during thermal ALE of Si(100) and LPCVD Si_3N_4 using the oxidation and "conversion-etch" mechanism.[36,37] The O_2-TMA-HF reactant sequence displayed a lower etch rate compared with the O_2-HF-TMA reactant sequence. The difference in etch rates is believed to be related to the favorability of TMA exposures following the HF exposures. TMA can undergo ligand-exchange with the fluoride surface layer after HF exposures. In contrast, TMA exposures after the O_2 exposures could lead to additional Al_2O_3 growth that may reduce the Al_2O_3 removal and slow the SiGe etch rate.

G. Etch selectivity of SiGe vs Si_3N_4 and Si

The selective etch of SiGe would be useful to fabricate Si nanowires and nanosheets using SiGe as the sacrificial layer.[7] Figure 12 shows the etching results for Si(100), LPCVD Si_3N_4, and

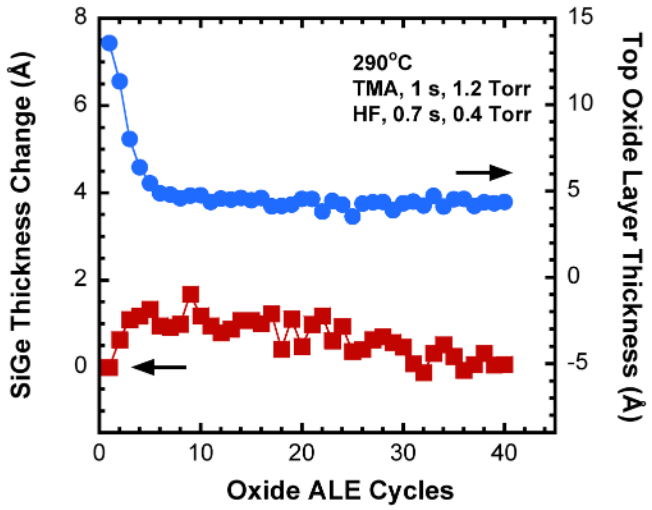

FIG. 10. Surface oxide thickness and SiGe thickness change as a result of surface oxide removal using sequential doses of TMA and HF at 290 °C.

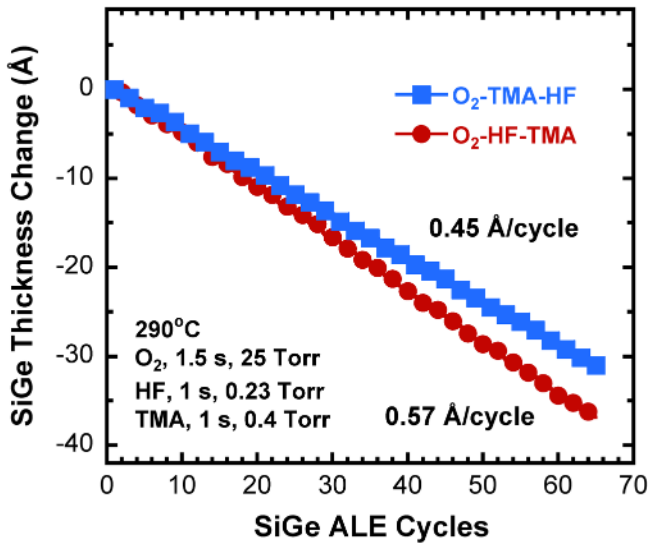

FIG. 11. SiGe thickness change vs number of ALE cycles for the O_2-HF-TMA and O_2-TMA-HF exposure sequences at 290 °C.

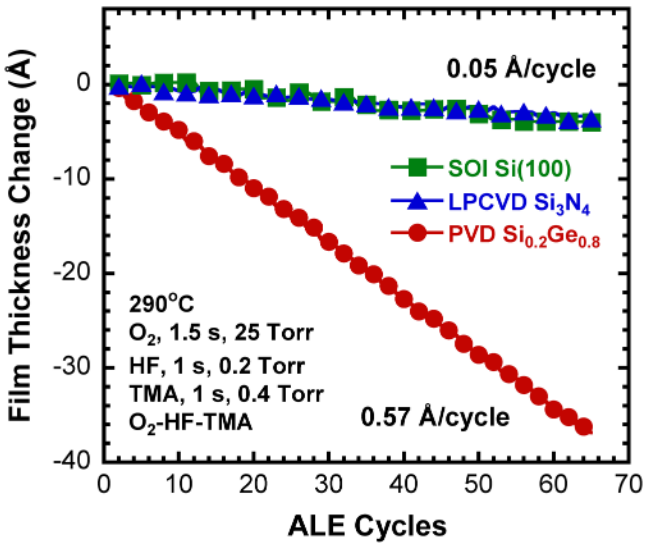

FIG. 12. Si, Si_3N_4, and SiGe film thickness changes vs the number of ALE cycles for the O_2-HF-TMA exposure sequence at 290 °C.

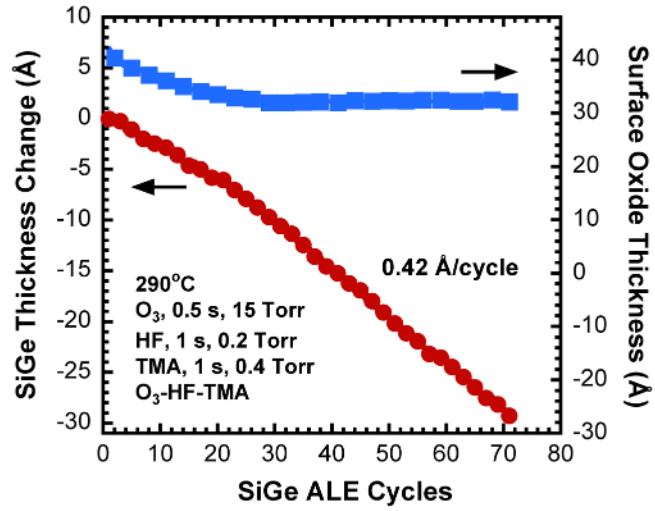

FIG. 13. SiGe thickness change and surface oxide film thickness vs the number of ALE cycles using sequential exposures of O_3, HF, and TMA at 290 °C.

SiGe films using the O_2-HF-TMA reactant sequence. The film thickness changes were measured in three separate runs using the same reaction conditions at 290 °C. O_2, HF, and TMA were dosed for 1.5, 1.0, and 1.0 s, respectively, with 30 s purge times between each reactant dose. These doses produced partial pressures of 25, 0.20, and 0.40 Torr for O_2, HF, and TMA, respectively.

Figure 12 demonstrates that the etch rate for the SiGe film is much faster than the etch rates for the Si and Si_3N_4 films at 290 °C. The SiGe film has an etch rate of 0.57 Å/cycle. In contrast, the Si and Si_3N_4 films display an etch rate of 0.05 Å/cycle. The SiGe etch rate is >10 times higher than the etch rate for Si or Si_3N_4. The selective etching of SiGe in the presence of Si is needed for the formation of Si nanowires and nanosheets for nanotransistor structures.[7]

H. SiGe thermal ALE using O_3

O_3 may also be an effective oxidation reactant for SiGe thermal ALE. Figure 13 shows the SiGe thickness change and surface oxide thickness versus the number of ALE cycles at 290 °C using an O_3-HF-TMA reactant sequence. The dose times of O_3, HF, and TMA were 0.5, 1.0, and 1.0 s, respectively. Partial pressures during the O_3, HF, and TMA doses were 15, 0.2, and 0.4 Torr, respectively. The purge time after each reactant exposure was 30 s. After a nucleation period of about 20 ALE cycles, the SiGe thickness decreased linearly with a rate of 0.42 Å/cycle. The surface oxide thickness also leveled out at about 32 Å after ~25 ALE cycles.

The SiGe etch rate of 0.42 Å/cycle using O_3 in the O_3-HF-TMA reactant sequence is similar to the SiGe etch rate of 0.57 Å/cycle using O_2 in the O_2-HF-TMA reactant sequence as obtained from Fig. 3. Direct comparison of the SiGe etch rates is difficult because the O_3 and O_2 pressures and dose times were different. Comparable etch rates with O_3 were also observed during Si and Si_3N_4 ALE when O_2 was replaced with O_3.[36,37] The surface oxide thickness of ~32 Å using O_3 is larger than the surface oxide thickness of ~19 Å using O_2 as shown in Fig. 3. Larger surface oxide thicknesses are expected for O_3 because ozone is a more powerful oxidizer than O_2.

The larger surface oxide thickness when using O_3 in the O_3-HF-TMA reactant sequence is consistent with thermochemical calculations. The standard Gibbs free energy changes for the reaction of O_3 with Si and Ge are[42]

$$Si + 1/1.5O_3(g) \rightarrow SiO_2; \qquad \Delta G^\circ(300\,^\circ C) = -222 \text{ kcal/mol}, \quad (5)$$

$$Ge + 1/1.5O_3(g) \rightarrow GeO_2; \qquad \Delta G^\circ(300\,^\circ C) = -141 \text{ kcal/mol}. \quad (6)$$

In comparison, the standard Gibbs free energy changes for the reaction of O_2 with Si and Ge are $\Delta G^\circ(300\,^\circ C) = -193$ kcal/mol and $\Delta G^\circ(300\,^\circ C) = -112$ kcal/mol for Si and Ge, respectively, as given in Eqs. (1) and (2). The larger standard Gibbs free energy changes may lead to larger surface oxide thicknesses.

I. Effect of reactant exposure

Figure 14 displays SiGe etch rate versus O_3, TMA, and HF dose times using an O_3-HF-TMA reactant sequence at 290 °C. A purge time of 30 s was used between the reactant doses. Figure 14(a) shows the change in the SiGe etch rate versus O_3 dose times from 0.5 to 2.0 s. The O_3 partial pressure increased from 15 Torr for the 0.5 s dose to 26 Torr for the 2.0 s dose. The TMA and HF dose times were fixed at 1 s. The partial pressures of TMA and HF were constant at 0.4 and 0.2 Torr, respectively. The results in Fig. 14(a) demonstrate that the O_3 reaction is self-limiting and independent of O_3 dose time and pressure for O_3 dose times >0.5 s.

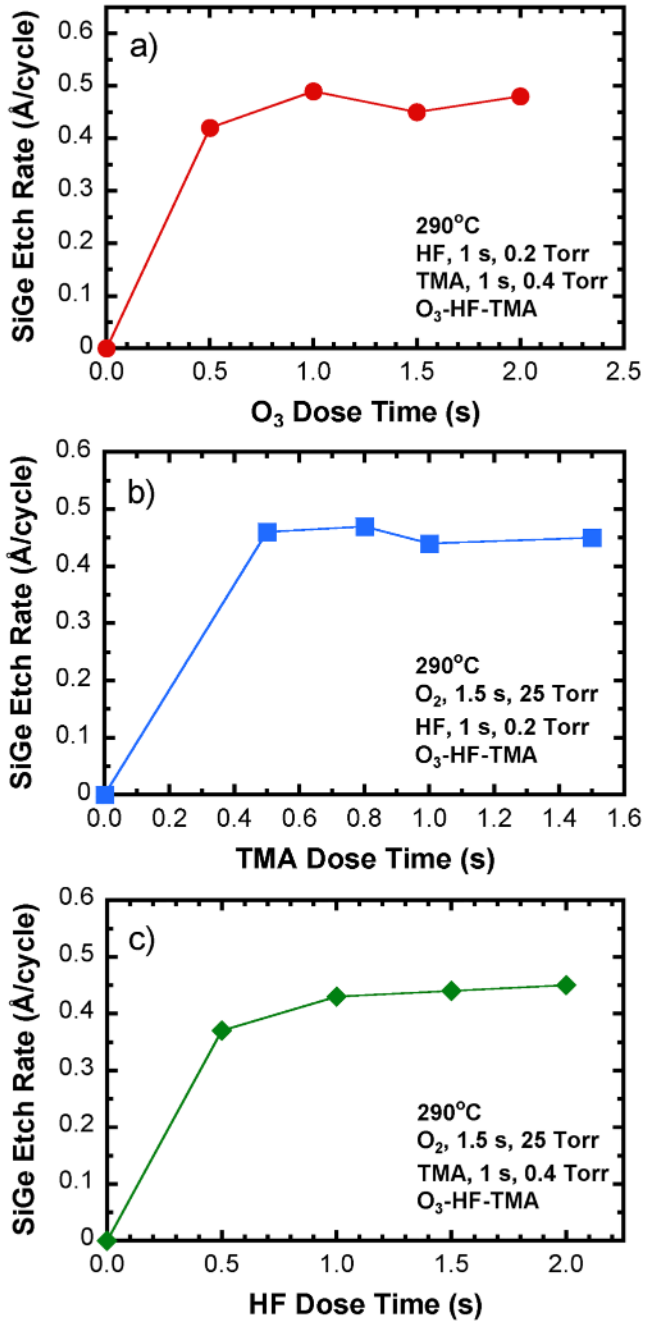

FIG. 14. SiGe etch rate vs (a) O_3, (b) TMA, and (c) HF dose times at 290 °C.

The SiGe etch rate versus O_3 exposure is more self-limiting than the SiGe etch rate versus O_2 exposure shown in Fig. 4(a). This behavior could be attributed to the higher oxidation power of O_3 compared with O_2. A comparison of Figs. 3 and 13 indicates that O_3 forms a thicker surface oxide layer than O_2. This thicker surface oxide layer could act as a more effective diffusion barrier layer to prevent progressive oxidation.[69]

Figure 14(b) shows the SiGe etch rates versus TMA dose time. The TMA dose times varied from 0.5 to 1.5 s while the O_3 and HF dose times were 1.5 and 1.0 s, respectively. The TMA reaction is self-limiting for TMA dose times >0.5 s. Figure 14(c) presents the SiGe etch rate versus HF dose time. The HF dose times varied between 0.5 and 2.0 s while the O_3 and TMA dose times were 1.5 and 1 s, respectively. In similarity with the results for O_3 and TMA, the HF reaction is self-limiting for HF dose times >0.5 s. The partial pressures of TMA and HF did not vary with increased dose times in Figs. 14(b) and 14(c).

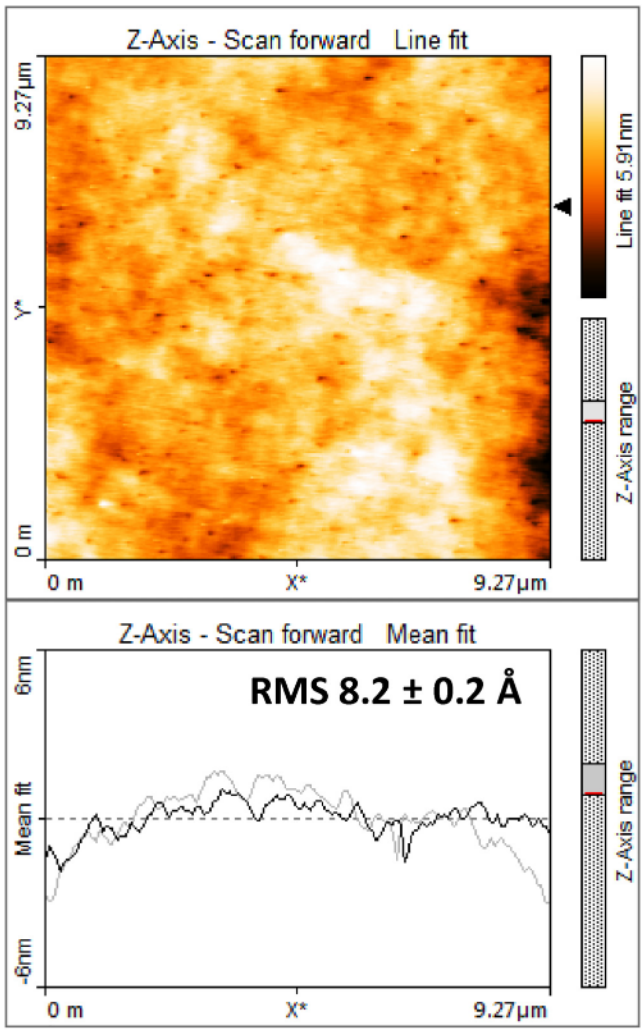

FIG. 15. AFM image of $Si_{0.15}Ge_{0.85}$ film surface after 100 ALE cycles using the O_3-HF-TMA dose sequence at 290 °C.

J. Surface roughness after etching

Figure 15 shows the AFM image of the $Si_{0.15}Ge_{0.85}$ film after 100 ALE cycles at 290 °C using O_3 as the oxidant. The etching was conducted using the O_3-HF-TMA reactant sequence with O_3, HF, and TMA dose times of 1.5, 1.0, and 1.0 s, respectively. The AFM measurements indicate that the RMS surface roughness after 100 ALE cycles is 8.2 ± 0.2 Å. This surface roughness is similar to the RMS surface roughness of 8.3 ± 0.2 obtained for the initial $Si_{0.15}Ge_{0.85}$ film in Fig. 7(a). This result is a slight improvement compared with the small RMS surface roughness increase to 9.5 ± 0.2 Å observed when using O_2 in the O_2-HF-TMA reaction sequence in Fig. 7(b).

IV. CONCLUSIONS

The thermal ALE of SiGe was studied using an oxidation and "conversion-etch" mechanism with either an O_2-HF-TMA or O_3-HF-TMA reactant sequence. The SiGe sample was a crystalline germanium-rich $Si_{0.15}Ge_{0.85}$ film. The SiGe film thickness and the surface oxide layer thickness on the SiGe film were both monitored during thermal ALE using *in situ* spectroscopic ellipsometry. The ellipsometric analysis measured a temperature-dependent etch rate from 225 to 290 °C. The maximum etch rate was measured at 290 °C, where the SiGe film thickness decreased linearly at a rate of 0.57 Å/cycle. During this SiGe thermal ALE, the surface oxide thickness was constant at ∼19 Å.

Additional experiments using the O_2-HF-TMA reaction sequence revealed that the TMA and HF reactions were self-limiting and the O_2 reaction was reasonably self-limiting at 290 °C. Atomic force microscopy images revealed that thermal ALE with the O_2-HF-TMA reaction sequence did not roughen the SiGe film. SiGe thermal ALE was also very selective to SiGe compared with Si or Si_3N_4 using the O_2-HF-TMA reaction sequence. The etch rate for the SiGe film was >10 times faster than Si(100) or Si_3N_4 at 290 °C.

Comparable etch rates were measured using an O_3-HF-TMA reaction sequence. The etch rate for SiGe was 0.42 Å/cycle at 290 °C. The O_3, TMA, and HF reactions were all self-limiting at 290 °C. In addition, atomic force microscopy images showed that the SiGe film was not roughened by thermal ALE with O_3-HF-TMA reaction sequences. Thermal ALE of SiGe using the oxidation and conversion-etch mechanism should be useful to fabricate SiGe devices. In addition, thermal ALE of SiGe could be employed to form Si nanowires and Si nanosheets using SiGe as the sacrificial layer.

ACKNOWLEDGMENTS

This research was funded by the Advanced Industries Accelerator (AIA) Program administered by the State of Colorado. The experimental apparatus was funded by the Defense Advanced Projects Agency (DARPA) under Grant No. W911NF-13-1-0041. The authors acknowledge Andrew Tomaschke at the University of Colorado at Boulder for providing the Raman results. In addition, the authors also thank Ryan Thorpe from Rutgers University for the RBS and FRES data and data analysis.

DATA AVAILABILITY

The data that support the findings of this study are available within the article.

REFERENCES

[1]S. M. George, Chem. Rev. **110**, 111 (2010).
[2]K. J. Kanarik, T. Lill, E. A. Hudson, S. Sriraman, S. Tan, J. Marks, V. Vahedi, and R. A. Gottscho, J. Vac. Sci. Technol. A **33**, 020802 (2015).
[3]S. M. George, Acc. Chem. Res. **53**, 1151 (2020).
[4]S. M. George and Y. Lee, ACS Nano **10**, 4889 (2016).
[5]G. S. Oehrlein, D. Metzler, and C. Li, ECS J. Solid State Sci. Technol. **4**, N5041 (2015).
[6]Y. Lee and S. M. George, ACS Nano **9**, 2061 (2015).
[7]H. H. Radamson *et al.*, Nanomaterials **10**, 1555 (2020).
[8]K. J. Kuhn, A. Murthy, R. Kotlyar, and M. Kuhn, ECS Trans. **33**, 3 (2010).
[9]M. V. Fischetti and S. E. Laux, J. Appl. Phys. **80**, 2234 (1996).
[10]M. L. Lee, E. A. Fitzgerald, M. T. Bulsara, M. T. Currie, and A. Lochtefeld, J. Appl. Phys. **97**, 011101 (2005).
[11]N. Singh, K. D. Buddharaju, S. K. Manhas, A. Agarwal, S. C. Rustagi, G. Q. Lo, N. Balasubramanian, and D. L. Kwong, IEEE Trans. Electron Devices **55**, 3107 (2008).
[12]D. Guo, G. *et al.* "FINFET technology featuring high mobility SiGe channel for 10 nm and beyond," *IEEE Symposium on VLSI Technology*, Honolulu, HI, June 14–16, 2016 (2016).
[13]E. Kawakami *et al.*, Nat. Nanotechnol. **9**, 666 (2014).
[14]E. M. T. Fadaly *et al.*, Nature **580**, 205 (2020).
[15]J. M. Ramirez *et al.*, Opt. Express **26**, 870 (2018).
[16]V. Vakarin *et al.*, Opt. Lett. **42**, 3482 (2017).
[17]S. Sedky, Microelectron. Eng. **84**, 2491 (2007).
[18]F. S. Johnson, D. S. Miles, D. T. Grider, and J. J. Wortman, J. Electron. Mater. **21**, 805 (1992).
[19]B. Hollander, D. Buca, S. Mantl, and J. M. Hartmann, J. Electrochem. Soc. **157**, H643 (2010).
[20]Y. Bogumilowicz, J. M. Hartmann, R. Truche, Y. Campidelli, G. Rolland, and T. Billon, Semicond. Sci. Technol. **20**, 127 (2005).
[21]J. M. Hartmann, V. Destefanis, G. Rabille, and S. Monfray, Semicond. Sci. Technol. **25**, 105009 (2010).
[22]N. Loubet, T. Kormann, G. Chabanne, S. Denorme, and D. Dutartre, Thin Solid Films **517**, 93 (2008).
[23]S. Borel, C. Arvet, J. Bilde, S. Harrison, and D. Louis, Microelectron. Eng. **73-4**, 301 (2004).
[24]V. Caubet, C. Beylier, S. Borel, and O. Renault, J. Vac. Sci. Technol. B **24**, 2748 (2006).
[25]J. J. Li *et al.*, J. Mater. Sci.: Mater. Electron. **31**, 134 (2020).
[26]E. Pargon, C. Petit-Etienne, L. Youssef, G. Thomachot, and S. David, J. Vac. Sci. Technol. A **37**, 040601 (2019).
[27]J. W. DuMont, A. E. Marquardt, A. M. Cano, and S. M. George, ACS Appl. Mater. Interfaces **9**, 10296 (2017).
[28]A. M. Cano, A. E. Marquardt, J. W. DuMont, and S. M. George, J. Phys. Chem. C **123**, 10346 (2019).
[29]Y. Lee, J. W. DuMont, and S. M. George, Chem. Mater. **28**, 2994 (2016).
[30]J. W. Clancey, A. S. Cavanagh, J. E. T. Smith, S. Sharma, and S. M. George, J. Phys. Chem. C **124**, 287 (2020).
[31]Y. Lee, J. W. DuMont, and S. M. George, ESC J. Solid State Sci. Technol. **4**, N5013 (2015).
[32]Y. Lee and S. M. George, J. Vac. Sci. Technol. A **36**, 061504 (2018).
[33]Y. Lee and S. M. George, J. Phys. Chem. C **123**, 18455 (2019).
[34]N. R. Johnson and S. M. George, ACS Appl. Mater. Interfaces **9**, 34435 (2017).
[35]D. R. Zywotko and S. M. George, Chem. Mater. **29**, 1183 (2017).
[36]A. I. Abdulagatov and S. M. George, Chem. Mater. **30**, 8465 (2018).
[37]A. I. Abdulagatov and S. M. George, J. Vac. Sci. Technol. A **38**, 022607 (2020).

[38]M. Tada, J. H. Park, J. R. Jain, and K. C. Saraswat, J. Electrochem. Soc. **156**, D23 (2009).
[39]M. I. Alonso and K. Winer, Phys. Rev. B **39**, 10056 (1989).
[40]T. R. Gow, R. Lin, L. A. Cadwell, F. Lee, A. L. Backman, and R. I. Masel, Chem. Mater. **1**, 406 (1989).
[41]T. M. Mayer, J. W. Rogers, and T. A. Michalske, Chem. Mater. **3**, 641 (1991).
[42]HSC Chemistry 10, Outokumpu Research Oy, Pori, Finland.
[43]M. A. Rabie, Y. M. Haddara, and J. Carette, J. Appl. Phys. **98**, 074904 (2005).
[44]P. E. Hellberg, S. L. Zhang, F. M. dHeurle, and C. S. Petersson, J. Appl. Phys. **82**, 5773 (1997).
[45]K. Kita, S. Suzuki, H. Nomura, T. Takahashi, T. Nishimura, and A. Toriumi, Jpn. J. Appl. Phys. **47**, 2349 (2008).
[46]S. K. Wang, K. Kita, C. H. Lee, T. Tabata, T. Nishimura, K. Nagashio, and A. Toriumi, J. Appl. Phys. **108**, 054104 (2010).
[47]D. A. Hansen and J. B. Hudson, Surf. Sci. **292**, 17 (1993).
[48]R. Zhang, T. Iwasaki, N. Taoka, M. Takenaka, and S. Takagi, Appl. Phys. Lett. **98**, 112902 (2011).
[49]W. K. Choi, L. K. Teh, L. K. Bera, W. K. Chim, A. T. S. Wee, and Y. X. Jie, J. Appl. Phys. **91**, 444 (2002).
[50]K. Tao, J. Wang, S. Jiang, R. Jia, Z. Jin, and X. Y. Liu, CrystEngComm **21**, 6623 (2019).
[51]M. H. Kibel and P. W. Leech, Surf. Interface Anal. **24**, 605 (1996).
[52]D. Schmeisser, R. D. Schnell, A. Bogen, F. J. Himpsel, D. Rieger, G. Landgren, and J. F. Morar, Surf. Sci. **172**, 455 (1986).
[53]K. Prabhakaran and T. Ogino, Surf. Sci. **325**, 263 (1995).
[54]V. Grossi, L. Ottaviano, S. Santucci, and M. Passacantando, J. Non-Cryst. Solids **356**, 1988 (2010).
[55]F. Bellenger, M. Houssa, A. Delabie, V. V. Afanas'ev, T. Conard, M. Caymax, M. Meuris, K. De Meyer, and M. M. Heyns, J. Electrochem. Soc. **155**, G33 (2008).
[56]G. Hollinger and F. J. Himpsel, J. Vac. Sci. Technol. A **1**, 640 (1983).
[57]G. Hollinger and F. J. Himpsel, Appl. Phys. Lett. **44**, 93 (1984).
[58]I. M. Lee and C. G. Takoudis, J. Vac. Sci. Technol. A **15**, 3154 (1997).
[59]M. R. Arghavani, R. Braunstein, G. Chalmers, D. Shirun, and P. Yang, Solid State Commun. **71**, 599 (1989).
[60]F. Fracassi, R. D'Agostino, A. Fornelli, and T. Shirafuji, Jpn. J. Appl. Phys., Part 1 **41**, 6287 (2002).
[61]O. Bose, E. Kemnitz, A. Lippitz, and W. E. S. Unger, Fresenius J. Anal. Chem. **358**, 175 (1997).
[62]A. E. Hughes, M. M. Hedges, and B. A. Sexton, J. Mater. Sci. **25**, 4856 (1990).
[63]A. Hess, E. Kemnitz, A. Lippitz, W. E. S. Unger, and D. H. Menz, J. Catal. **148**, 270 (1994).
[64]K. Roodenko, M. D. Halls, Y. Gogte, O. Seitz, J. F. Veyan, and Y. J. Chabal, J. Phys. Chem. C **115**, 21351 (2011).
[65]B. H. Liao, C. N. Hsiao, and C. C. Lee, Opt. Mater. Express **6**, 1506 (2016).
[66]M. C. Peignon, C. Cardinaud, G. Turban, C. Charles, and R. W. Boswell, J. Vac. Sci. Technol. A **14**, 156 (1996).
[67]H. Yao, J. A. Woollam, and S. A. Alterovitz, Appl. Phys. Lett. **62**, 3324 (1993).
[68]K. Utani, T. Suzuki, and S. Adachi, J. Appl. Phys. **73**, 3467 (1993).
[69]B. E. Deal and A. S. Grove, J. Appl. Phys. **36**, 3770 (1965).